

The infrared spectra of ABC-stacking tri- and tetra-layer graphenes studied by first-principles calculations

Yuehua Xu¹ and San-Huang Ke^{1,*}

¹*Department of Physics, Tongji University, 1239 Siping Road, Shanghai 200092, P. R. of China*

The infrared absorption spectra of ABC-stacking tri- and tetra-layer graphenes are studied using the density functional theory. It is found that they exhibit very different characteristic peaks compared with those of AB-stacking ones, caused by the different stacking sequence and interlayer coupling. The anisotropy of the spectra with respect to the direction of the light electric field is significant. The spectra are more sensitive to the stacking number when the electric field is perpendicular to the graphene plane due to the interlayer polarization. The high sensitivities make it possible to identify the stacking sequence and stacking number of samples by comparing theory and experiment.

I. INTRODUCTION

Single-layer graphene (SG) is a two-dimensional (2D) flat monolayer composed of carbon atoms arranged in a honeycomb network, which is a basic building block for all other graphite materials. In the past, it was believed to be unstable in free-standing state [1] and so described as an 'academic' material. However, SG was unexpectedly made experimentally several years ago [2]. The unique electronic properties of SG is mainly due to its very peculiar band structure, with the π and π^* bands showing linear dispersion around the Fermi level (E_F) where they touch with each other at a single point K in the Brillouin zone (BZ) [3, 4]. Because of its great potential for applications in nano-science and technology, SG has been thoroughly studied both theoretically and experimentally [5–10].

Recently, a further progress in this field was the successful fabrication and use of few-layer graphenes (FGs) which are stacking of a few graphene layers [11–13]. From the viewpoint of application, FGs can be even more useful than SG since it offers further control of electronic states by interlayer interactions [14–18], or by applying an electric field perpendicular to the molecular plane to open a band gap which is critical for applications in nanoelectronics [19, 20]. Because of the interlayer interaction, theoretically, there can be dramatic changes in the electronic properties of FGs compared with those of SG, depending on the stacking sequence and number (N). Considering an arbitrary arrangement for adjacent graphene layers, there will be 2^{N-2} possible low-energy stacking sequences for FGs of N layers. It is therefore desirable and important to understand the electronic properties of the different FGs and to be able to identify accurately their stacking sequence and number. Experimentally, infrared (IR) absorption spectra can be used to obtain the detailed information about the low-energy electronic excitations in FGs. If one has the knowledge about the influence of different stacking sequences and numbers on the IR absorption spectra, one can identify them accurately in terms of the experimental IR spectra. This knowledge can be obtained from theoretical calculations, especially from first-principles calculations which have

the advantage of being empirical parameter free and therefore having the predictive power.

Motivated by the fact that natural graphite adopts the AB-stacking (Bernal) sequence [21] which gives the lowest total energy, many theoretical and experimental studies in the past few years were focusing on the electronic and optical properties of AB-stacking FGs [22–27], especially their infrared absorption spectra [28–30]. For example, it was found that the interlayer coupling in an AB-stacking bilayer graphene (BG) leads to remarkable changes in its low-energy dispersions as well as its IR spectra compared with those of SG [12, 31–34]. On the other hand, very recently, ABC-stacking (rhombohedral) FGs were also found experimentally. For example, Norimatsu *et al* observed selective formation of ABC-stacking graphene layers [35], and more recently, Mak *et al* reported unambiguous experimental evidence for the existence of stable tetra-layer graphenes in both AB- and ABC-stacking sequences [36]. The existence of these stable polytypes of FG provides a new possible way to tailor the electronic structure of FGs materials for both fundamental studies and application interests [37–40]. However, because of the lack of practical samples and related experimental observation in the past, theoretical studies on the band structure and optical properties, especially the IR absorption spectra, of the ABC-stacking sequence are still very limited [41–45], except for some simplified tight-binding (TB) modeling [46, 47].

In this paper, we study the electronic structures and IR absorption spectra of ABC-stacking tri- and tetra-layer graphenes (for simplicity, we call them ABC-3 and ABC-4, respectively) using first-principles density functional theory (DFT) calculations. The low-energy band dispersion and the formation of the characteristic peaks in their IR absorption spectra are analyzed in comparison with those of the AB-stacking ones (called AB-3 and AB-4, respectively), showing significant effects from the stacking sequence. The anisotropy of the spectra with respect to the direction of the light electric field is also investigated and is found to be remarkable. Our theoretical results for AB-4 and ABC-4 are in good agreement with an very recent experimental report [36]. Compared to TB model calculations, the present calculation has the advantage of better transferability and predictive power since it is free of any empirical parameter. We show that, together with reliable experimental data, the theoretical calculation of IR spectra can provide a useful tool for identifying the stacking sequence and

*Corresponding author, E-mail: shke@tongji.edu.cn

even the stacking number of samples. The rest part of our paper is arranged as follows: In the next section (Section II) we give briefly the theory and computational details; We discuss the results in Section III, followed by a summary in Section IV .

II. THEORY AND COMPUTATIONAL DETAILS

A. IR optical absorption

The ground-state electronic structure of a FG can be calculated using density functional theory. After the band structure $E(\mathbf{k}, j)$ and corresponding eigenfunctions are obtained, its IR absorption properties can be studied by looking at the imaginary part of the frequency-dependent dielectric function [48]:

$$\begin{aligned} \epsilon_2^{\alpha\beta}(\omega) = & \frac{(2\pi e)^2}{\Omega} \lim_{q \rightarrow 0} \frac{1}{q^2} \sum_{j_1, j_2, \mathbf{k}} 2w_{\mathbf{k}} \\ & \times \langle u_{j_1, \mathbf{k} + \mathbf{e}_{\alpha} q} | u_{j_2, \mathbf{k}} \rangle \langle u_{j_1, \mathbf{k} + \mathbf{e}_{\beta} q} | u_{j_2, \mathbf{k}} \rangle^* \\ & \times \delta [E(\mathbf{k}, j_1) - E(\mathbf{k}, j_2) - \omega], \end{aligned} \quad (1)$$

where ω and q are the energy and momentum of photon, respectively; Ω denotes the volume of the unit cell; e is the charge of electron and $w_{\mathbf{k}}$ is the weight of \mathbf{k} -point \mathbf{k} for the \mathbf{k} -sampling; Indices $j_1 = 1, 2, \dots, N$ and $j_2 = -1, -2, \dots, -N$ denote the conduction and valence subbands, respectively, counted from the Fermi level; $u_{j, \mathbf{k}}$ is the cell periodic part of the wavefunction of band j at \mathbf{k} -point \mathbf{k} . Under an electric field parallel to the graphene plane ($\mathbf{E} \parallel \mathbf{x}$ or $\mathbf{E} \parallel \mathbf{y}$) or perpendicular to the graphene plane ($\mathbf{E} \parallel \mathbf{z}$) which is studied in our work, the electrons could be excited from the occupied valence π bands to the unoccupied conduction π^* bands. At zero temperature, only inter- π -band excitations can occur with the excitation energy $\omega_{\text{ex}} = E(\mathbf{k}, j_1) - E(\mathbf{k}, j_2)$. Because photon's momentum is almost zero, the optical selection rules is $\Delta \mathbf{k} = 0$.

B. Computational details

For band structure calculation, we use the density functional theory implemented in the plane-wave pseudopotential formalism [49] with the local density approximation (LDA) in the Ceperley-Alder version [50] for the electron exchange and correlation. The interaction between the ions and electrons is described by the highly accurate full-potential projected augmented wave (PAW) method [51, 52] which can give a more accurate and reliable result than the ultrasoft pseudopotential. In our calculations, the $2s$ and $2p$ orbitals of the carbon atoms are treated as valence orbitals, and a large plane-wave cutoff of 500 eV is used throughout. A uniform grid larger than $200 \times 200 \times 1$ is used in the irreducible BZ for the \mathbf{k} -sampling.

A supercell geometry is constructed so that the tri- and tetra-layer graphenes are aligned in a hexagonal supercell with the closest distance between the adjacent FGs being at least

10\AA along the stacking direction (\mathbf{z} direction). The interlayer spacing is set initially to be the same as in graphite. The structures of ABC-3 and AB-3 are shown in Figs. 1(a) and 1(b), respectively, where there exist two C atoms, denoted by A_i and B_i , in a primitive cell of each graphene layer i . The two polytypes can be obtained by displacing each adjacent graphene layer continuously in one direction for the ABC stacking, and alternatively in opposite direction for the AB stacking. We use a conjugated gradient method to optimize the atom's positions as well as the size of the supercell until the forces acting on all the atoms are less than $0.005 \text{ eV}/\text{\AA}$. With the obtained equilibrium structure, we then use a more dense set of \mathbf{k} -points to calculate the electronic structure and the moment matrix elements. Finally we use the Eq. (1) to study the IR absorption properties.

III. RESULTS AND DISCUSSION

A. Atomic structure and energy band structure

The equilibrium C-C bond length a given by the DFT-LDA structural optimization calculation is 1.41\AA for both the ABC- and AB-stacking FGs, which is almost the same as that in bulk graphite. However, the interlayer spacing b is slightly different for the different stacking sequences and stacking numbers: 3.31 and 3.32\AA for ABC-3 and ABC-4, respectively, and 3.32 and 3.34\AA for AB-3 and AB-4, respectively. Our result of 3.31\AA for ABC-3 is in good agreement with an available experimental value 3.335\AA [45], both are a bit smaller than the value 3.37\AA in ABC-stacking graphite [53].

The low-energy band dispersions of the four systems are given in Figs. 2 (a) - (d). Let's first look at the AB-stacking case (Figs. 2(a) and 2(c)). As is evident, the low-energy band structure consists of separate single-layer-like and bilayer-like bands [44] but with some degree of distortion due to the additional interlayer couplings. Meanwhile, the interlayer couplings reduce the symmetry between the valence and conduction bands with respect to the Fermi level, and also cause a small overlap between them near E_F . For example, for AB-3, our calculation predicts different energy splittings of -483 and $+552 \text{ meV}$ at the K point for the low-lying and up-lying bands, respectively. For AB-4, the above band splittings at the K point given by our calculation are -551 meV , -211 meV , 222 meV , 597 meV for the four bands (see Fig. 2(c)), respectively, while they are ± 222 and $\pm 596 \text{ meV}$ from a TB model calculation [36]. We note that our band structure is asymmetrical with respect to the Fermi level while the result of the TB model [36] is symmetrical. Based upon the previous experimental IR absorption spectra of doped or gated AB-stacking FGs [32, 54, 55], one can deduce that the valence and conduction bands are asymmetrical with respect to E_F . Our result for the AB stacking is consistent with the experimental data while the result given by the simplified TB model is not, indicating that our DFT-LDA band structure calculation is more reasonable than the TB model calculation.

For ABC-3 and ABC-4 which is the focus of our study, one can see in Figs. 2(b) and 2(d) that they have strikingly differ-

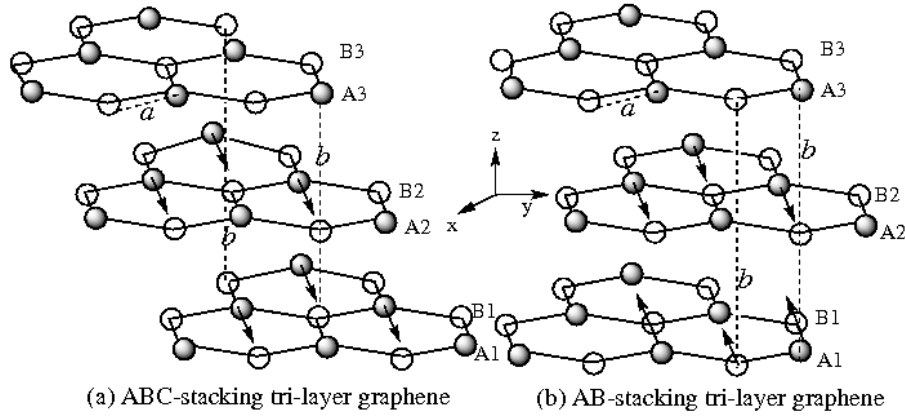


FIG. 1: Structures of tri-layer graphenes: (a) ABC-stacking, (b) AB-stacking. The C-C bond length is denoted by a and the interlayer spacing is denoted by b .

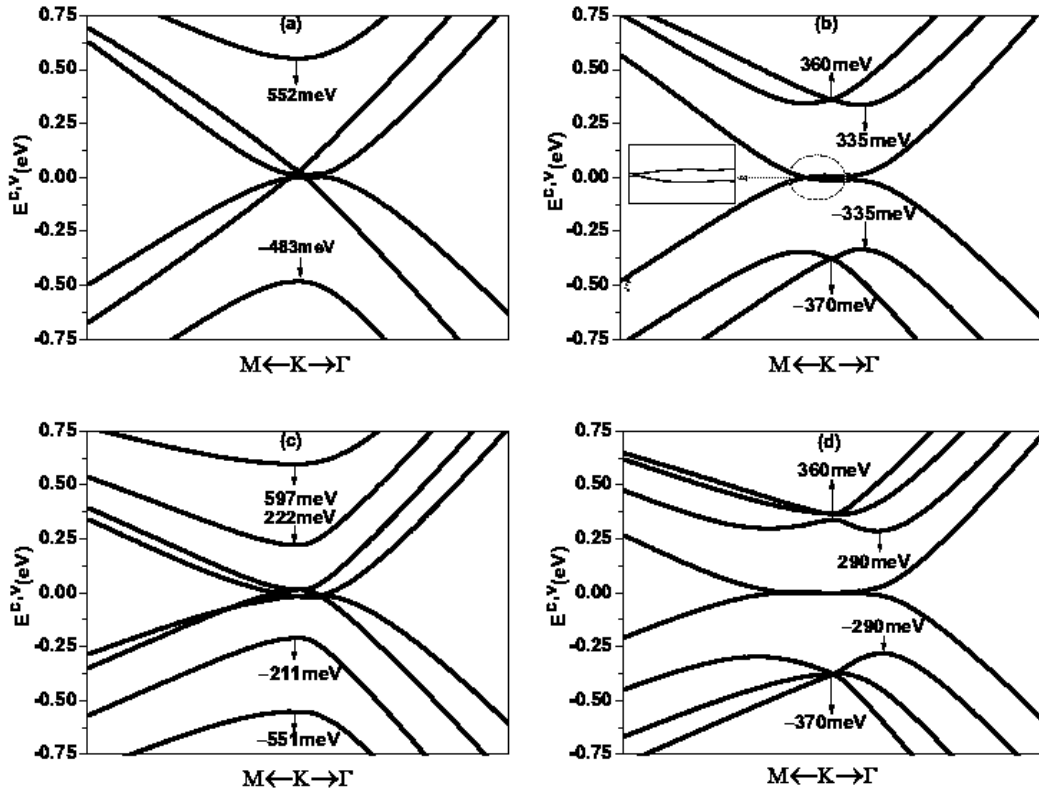


FIG. 2: The low-energy band dispersions of the four systems studied: (a) AB-3, (b) ABC-3, (c) AB-4, and (d) ABC-4, as used in the text.

ent 2D band structures from those of the AB-stacking ones, which reflect the underlying difference in crystallographic symmetry and interlayer coupling. First, unlike in the AB-stacking case, the band dispersions of the ABC-stacking FGs don't resemble those of single-layer and bilayer graphenes. The different interlayer interaction causes two intersections at the K point with the energy of $+360\text{meV}$ and -370meV , respectively, which are absent in AB-3 and AB-4. Again, here the band structure is slightly asymmetrical with respect to the Fermi level while it is symmetrical in some TB model calculations ($\pm 360\text{meV}$) [36, 37]. Second, the lower crystallographic

symmetry of the ABC-stacking shifts the extrema of the low-lying and up-lying energy bands away from the K point. In ABC-3 case, the four shifted extrema of these "wizad-hat" bands have energies of about 335meV away from E_F , as shown in Fig. 2(b), while in ABC-4 case they are about 290meV away from E_F . Third, the interlayer interactions produce one pair of localized flat bands near E_F . For ABC-3, the two flat bands have a tiny energy gap on the $K - \Gamma$ line while for ABC-4 they have a small overlap. Physically, these flat bands are formed by the localized electronic states from the two outermost graphene layers.

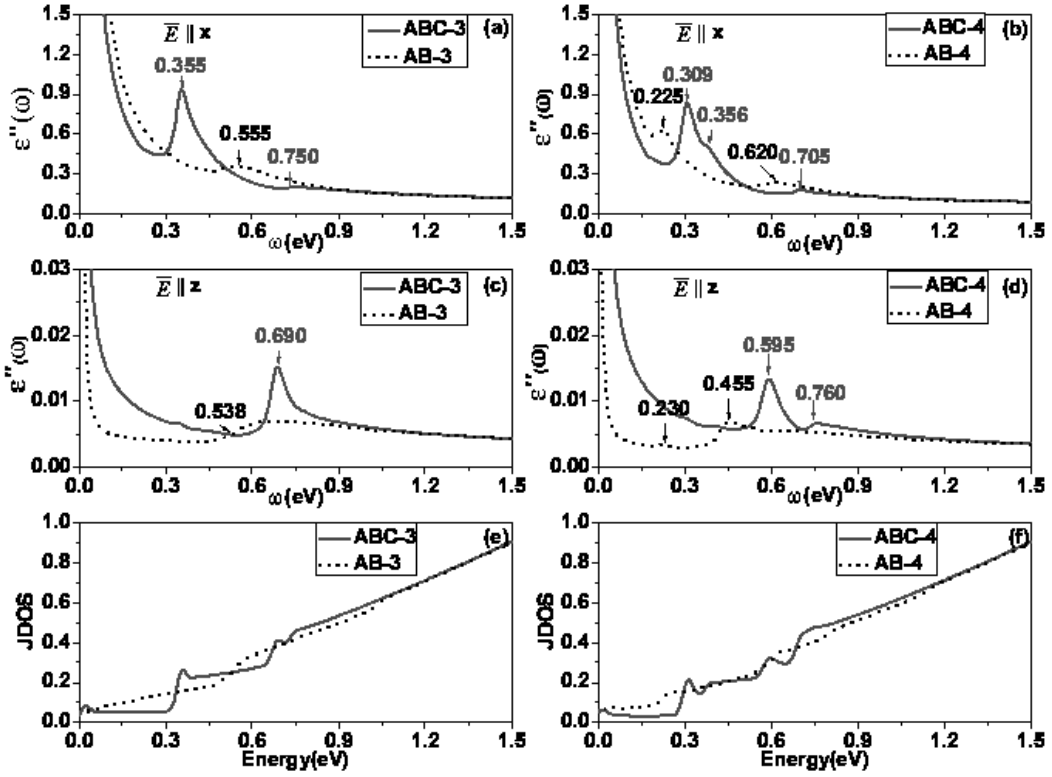


FIG. 3: Calculated IR absorption spectra of (a) ABC-3 and AB-3 under $\mathbf{E} \parallel \mathbf{x}$, (b) ABC-4 and AB-4 under $\mathbf{E} \parallel \mathbf{x}$, (c) ABC-3 and AB-3 under $\mathbf{E} \parallel \mathbf{z}$, and (d) ABC-4 and AB-4 under $\mathbf{E} \parallel \mathbf{z}$. The solid line is for ABC stacking and the dotted line is for AB stacking. The corresponding joint densities of states (JDOS) are shown in (e) and (f).

B. IR absorption spectra

We calculate the IR absorption spectra of the AB- and ABC-stacking tri- and tetra-layer FGs for two different directions of the light electric field ($\mathbf{E} \parallel \mathbf{x}$ and $\mathbf{E} \parallel \mathbf{z}$) and plot the results in Fig. 3 (a) - (d) together with the corresponding joint densities of states (JDOS) in Fig. 3(e) and (f). Let us start with the discussion about the different behavior between the ABC stacking (the solid lines in Fig. 3) and the AB stacking (the dotted lines). We first consider the case of $\mathbf{E} \parallel \mathbf{x}$. As one can see in Fig. 3(a), for AB-3 there exists one characteristic peak at 555 meV, which is mainly caused by the transitions between the valence bands $j_2 = -3$ (-1) and conduction bands $j_1 = 1$ (3) with their average energy difference being about 555 meV around the K point, denoted by the red arrows in Fig. 4(a). For ABC-3, on the other hand, its characteristic peak is located at 355 meV. This peak is due to the transitions between valence band $j_2 = -2$ (around the extremum) and conduction band $j_1 = 1$ as well as $j_2 = -1$ and $j_1 = 2$ (around the extremum) with their average energy difference being 355 meV, as denoted by the red arrows in Fig. 4(b). The corresponding peaks in the JDOS can be found in Fig. 3(e). For ABC-3 the peak at 355 meV in the JDOS is due to 1D-like van Hove singularity (vHS) which was analyzed earlier by a TB model 56 and ascribed to the fact that the "wizard-hat" bands have their extrema away from the K point. In addition, for ABC-3, there also exists another weak peak at 750 meV, which is mainly caused by transitions between the two inter-

sections around the K point, i.e., between the valence bands $j_2 = -2, -3$ and conduction bands $j_1 = 2, 3$. Obviously, the characteristic peak at 355 meV of ABC-3 has a red-shift of 200 meV compared with that at 555 meV of AB-3 while the peak at 750 meV of ABC-3 is absent in AB-3. For AB-4, as one can see in Fig. 3(b), there are two characteristic peaks, one at 225 meV and the other at 620 meV. The peak at 225 meV is mainly caused by the transitions between the valence bands $j_2 = -3$ (-3) and conduction bands $j_1 = 1$ (2) with the interlayer-coupling induced splitting energy between the pairs being about 225 meV, which are denoted by the red arrows in Fig. 4(c). The peak at 620 meV is due to the transitions between the valence bands $j_2 = -2, -1, -4$ and conduction bands $j_1 = 4, 4, 1$, respectively. For ABC-4, on the other hand, there is one major peak at 309 meV which is mainly caused by the transitions between the valence band $j_2 = -2$ (around the extremum) and conduction band $j_1 = 1$ as well as $j_2 = -1$ and $j_1 = 2$ (around the extremum) with the average energy difference 309 meV, denoted by the red arrows in Fig. 4(d). The corresponding peak in the JDOS (1D-like vHS) can be observed at around 309 meV in Fig. 3(f). Besides the major characteristic peak there also exist two weaker structures in the IR spectra of ABC-4. One is a "shoulder structure" at 356 meV, which is mainly caused by the transitions between the valence bands $j_2 = -3$ (-1) and conduction bands $j_1 = 1$ (3) around the K points. The other is a weaker peak at 705 meV which is induced by the transition between the intersections of the valence bands $j_2 = -2$ (-3) and conduction bands $j_1 = 3$ (2)

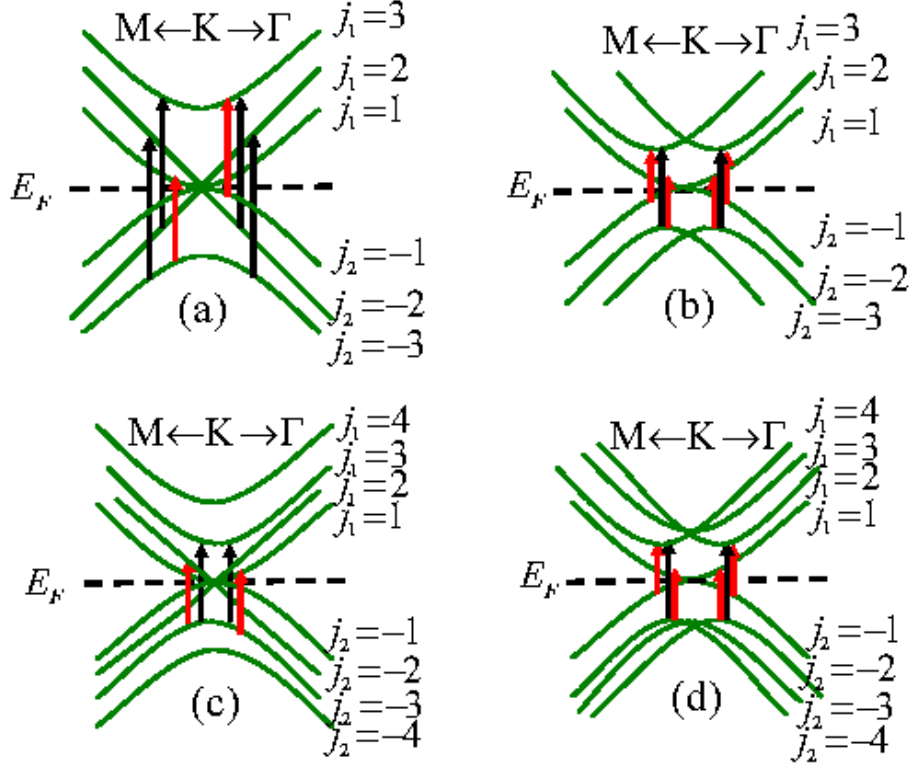


FIG. 4: Schematic drawing of the band structures of (a) AB-3, (b) ABC-3, (c) AB-4, and (d) ABC-4, which are in the same order as in Fig. 2. Red and black arrows denote different permitted optical transitions. Conduction bands are denoted by index j_1 and valence bands are denoted by index j_2 .

around the K points. Overall, the three structures in the IR spectrum of ABC-4 are blue-shifted with respect to the two structures of AB-4. Specifically, the major peak at 309 meV has a blue-shift of 84 meV with respect to the peak at 225 meV of AB-4. The weak peak at 705 meV of ABC-4 has a blue-shift of 85 meV with respect to the peak at 620 meV of AB-4. While the "shoulder structure" at 356 meV is absent in AB-4.

Next, we consider the case of $\mathbf{E} \parallel \mathbf{z}$ (see Figs. 3(c) and (d)). For AB-3, a jump lies at 538 meV, which is caused by transitions between valence bands $j_2 = -2$ (-3) and conduction bands $j_1 = 3$ (2) near the K point with their average energy difference being about 538 meV, denoted by the black arrows in Fig. 4(a). The corresponding jump structure in the JDOS can be seen in Fig. 3(e). In contrast, for ABC-3, a characteristic peak appears at 690 meV. The transitions behind are between the valence band $j_2 = -2$ (around the extremum) and conduction band $j_1 = 2$ (around the extremum) as well as $j_2 = -3$ and $j_1 = 3$, denoted by the black arrows in Fig. 4(b). This peak corresponds to the 1D-like vHS at 690 meV in the JDOS (see Fig. 3(e)), which is quite different from the 2D systems' characteristic jump structure (or call step singularity) at 538 meV of AB-3. For AB-4, as can be seen in Fig. 3(d), there is a weak peak at 230 meV and a major peak at 455 meV which is induced by the transition between $j_2 = -3$ and $j_1 = 3$, denoted by the black arrows in Fig. 4(c). In Fig. 3(f) one can see the corresponding features in the JDOS for these two peaks. For ABC-4, on the other hand, a major

peak is at 595 meV, as shown in Fig. 3(d), which is due to the transitions between the extrema of valence band $j_2 = -2$ and conduction band $j_1 = 2$, denoted by the black arrows in Fig. 4(d). The corresponding peak in the JDOS (1D-like vHS) is shown in Fig. 3(f). Another weaker peak at 760 meV (Fig. 3(d)) is caused by the transition between $j_2 = -3$ and $j_1 = 3$ around the K point. Overall, the peaks in the IR spectrum of ABC-4 are blue-shifted with respect to those of AB-4.

The different IR absorption behavior between the ABC- and AB-stacking FGs can be understood by considering the difference in their electronic structure. As mentioned previously, the ABC stacking has a lower crystallographic symmetry compared with the AB stacking. As a result, the extrema of its low- and up-lying energy bands are shifted away from the K point, which gives rise to the 1D-like vHS in their JDOS and prominent optical absorption peaks. These prominent peaks are in strong contrast with the much weaker intensity structures in the IR spectra of the AB stacking, and also located at very different frequencies.

So far, almost all experiments [32, 36, 54, 55] and theoretical TB model calculations [15, 46, 47] considered only the case of $\mathbf{E} \parallel \mathbf{x}$ in investigating the IR spectra of FGs, while the case of $\mathbf{E} \parallel \mathbf{z}$ was little concerned [34] although the setup of $\mathbf{E} \parallel \mathbf{z}$ is feasible in experiment and can provide more information, as already implied in our previous discussion. Below we discuss in more details the effect of different directions of the light electric field on the IR absorption spectra. It is evident from Fig. 3 that the IR absorption spectra show a

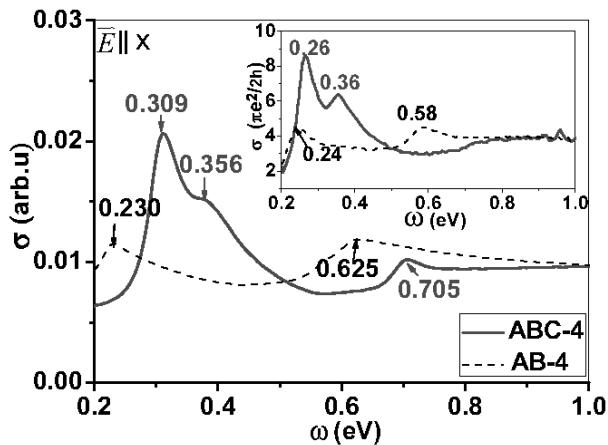


FIG. 5: IR optical conductivity spectra of ABC-4 (solid line) and AB-4 (dashed line) under $\mathbf{E} \parallel \mathbf{x}$. The inset shows the corresponding experimental results reported by Mak *et al* in Ref.[36]. The positions of the peaks are denoted.

strong anisotropy between $\mathbf{E} \parallel \mathbf{x}$ and $\mathbf{E} \parallel \mathbf{z}$. For ABC-3, the position of its major characteristic peak (at 690 meV) under $\mathbf{E} \parallel \mathbf{z}$ has a large blue-shift of 335 meV compared with the case of $\mathbf{E} \parallel \mathbf{x}$. In addition, there is a weak peak at 750 meV under $\mathbf{E} \parallel \mathbf{x}$, which is absent under $\mathbf{E} \parallel \mathbf{z}$. For AB-3 the peak at 555 meV under $\mathbf{E} \parallel \mathbf{x}$ is replaced by a jump, instead of a peak, around 538 meV, as shown in Fig. 3(c). Similar to the tri-layer systems, the tetra-layer systems also show a strong anisotropy effect between $\mathbf{E} \parallel \mathbf{x}$ and $\mathbf{E} \parallel \mathbf{z}$, particularly ABC-4: Its characteristic peaks are significantly blue-shifted from $\mathbf{E} \parallel \mathbf{x}$ to $\mathbf{E} \parallel \mathbf{z}$, by up to 286 meV. One thing to note is that, compared with the AB stacking, the ABC stacking has a much stronger anisotropy effect causing large blue-shifts for its major peaks from $\mathbf{E} \parallel \mathbf{x}$ to $\mathbf{E} \parallel \mathbf{z}$ (see Fig. 3 (a) vs. (c), and (b) vs. (d)). Physically, this can be understood also by considering its lower crystallographic symmetry which results in a very different band structure including the "wizard-hat" bands. This band structure provides two sets of transitions with significantly different transition energies for $\mathbf{E} \parallel \mathbf{x}$ and $\mathbf{E} \parallel \mathbf{z}$, respectively (see Fig. 4, red arrows vs. black arrows).

Finally, we would like to discuss how the number of stacking layers affects the IR spectra. As can be seen in Fig. 3, the thickness effect ((a) vs. (b) and (c) vs. (d)) is not so significant compared to the effect from stacking sequence. For the ABC stacking, all the characteristic peaks have a red-shift as the stacking number increases. For the AB stacking, however, the trend is not so clear. Under $\mathbf{E} \parallel \mathbf{x}$ the maximum shift in peak position is about 45meV between ABC-3 and ABC-4. This shift is enhanced to more than 90meV under $\mathbf{E} \parallel \mathbf{z}$. Physically, this enhanced effect can be understood by considering the interaction between the light electric field and the graphene sheets. In the former case the field will induce an intra-layer polarization which is less sensitive to the thickness while in the latter the field will induce an inter-layer polarization which is more sensitive to the thickness.

From our discussion, one can see that different stacking sequences of FGs have very significant effects on their IR ab-

sorption spectra, leading to peaks at different frequencies and with different intensities. Furthermore, our calculation shows that the IR spectra are also sensitive to the direction of the light electric field, especially for the ABC stacking sequence. In the case of $\mathbf{E} \parallel \mathbf{z}$ the thickness of an ABC-stacking sample also plays an important role. The high sensitivities of the IR absorption spectra to the different factors provide important information for identifying the stacking sequence and stacking number of an experimental sample by comparing the experimental spectra with the calculated ones. Below, we compare our theoretical result with an experimental report [36] which is, to the best of our knowledge, the only available one in literature for ABC-stacking FGs so far. In order to have a reasonable comparison, we plot the IR optical conductivity spectra $\sigma(\omega) = \omega\epsilon_2(\omega)/4\pi$ [57] in Fig. 5 for ABC-4 and AB-4 under $\mathbf{E} \parallel \mathbf{x}$. One can see that our theoretical results are in good overall agreement with the experiment data (see the inset in Fig. 5) for both ABC-4 and AB-4. The positions of the peaks and their relative intensities as well as the overall shape of the two experimental spectra are all well reproduced. Quantitatively, however, there are still some discrepancies between theory and experiment. For AB-4 the maximum difference in the peak position is about 45 meV while for ABC-4 it is up to 50 meV. Additionally, for ABC-4 our calculation predicts a weak peak at 705 meV, which was also found in the simplified TB's model calculation [36] but with a slight shift (670 meV). However, this peak was not observed in the experiment. How to understand these quantitative discrepancies is still an open problem. It may be due to some experimental environment which has not been taken into account in our DFT calculation, such as doping, disorder, defect effects. The experimentally missed peak at 705 meV, on the other hand, may be due to temperature broadening. To clarify the quantitative inconsistency between theory and experiment, further theoretical work and more experimental measurements are desirable.

IV. SUMMARY

We have studied the IR absorption spectra of ABC-stacking tri- and tetra-layer FGs using a first-principle method for two different directions of the light electric field ($\mathbf{E} \parallel \mathbf{x}$ and $\mathbf{E} \parallel \mathbf{z}$), and compare them with those of AB-stacking ones. The findings are as follows. 1) The ABC-stacking sequence causes great different band structures, inducing characteristic peaks at different positions and with different intensities, no matter $\mathbf{E} \parallel \mathbf{x}$ or $\mathbf{E} \parallel \mathbf{z}$. 2) The IR spectra show a strong anisotropy effect between $\mathbf{E} \parallel \mathbf{x}$ and $\mathbf{E} \parallel \mathbf{z}$. 3) The IR spectra are much more sensitive to the stacking number under $\mathbf{E} \parallel \mathbf{z}$ because of the induced inter-layer polarization. 4) Our calculated IR optical conductivity spectra for the tetra-layer graphenes under $\mathbf{E} \parallel \mathbf{x}$ are well consistent with a recent experimental observation. The significant effects of the different factors on the IR spectra of FGs provide useful tools for identifying their stacking sequence and stacking number.

This work was supported by Shanghai Pujiang Program under Grant 10PJ1410000 and the MOST 973 Project 2011CB922200.

-
- [1] E. Fradkin, Phys. Rev. B **33** (5), 3263 (1986).
- [2] K. S. Novoselov, A. K. Geim, S. V. Morozov, D. Jiang, Y. Zhang, S. V. Dubonos, I. V. Grigorieva, and A. A. Firsov, Science **306** (5696), 666 (2004).
- [3] A. K. Geim, Science **324** (5934), 1530 (2009).
- [4] Y. Zhang, Y.-W. Tan, H. L. Stormer, and P. Kim, Nature **438** (7065), 201 (2005).
- [5] C. Berger, Z. M. Song, T. B. Li, X. B. Li, A. Y. Ogbazghi, R. Feng, Z. T. Dai, A. N. Marchenkov, E. H. Conrad, P. N. First, and W. A. de Heer, J. Phys. Chem. B **108** (52), 19912 (2004).
- [6] C. P. Chang, C. L. Lu, F. L. Shyu, R. B. Chen, Y. K. Fang, and M. F. Lin, Carbon **42** (14), 2975 (2004).
- [7] X. F. Wang and T. Chakraborty, Phys. Rev. B **75** (4), 041404(R) (2007).
- [8] L. Joly, L. Tati-Bismaths, and W. Weber, Phys. Rev. Lett. **97** (18), 187404 (2006).
- [9] M. L. Sadowski, G. Martinez, M. Potemski, C. Berger, and W. A. de Heer, Phys. Rev. Lett. **97** (26), 266405 (2006).
- [10] E. McCann, Phys. Rev. B **74** (16), 161473 (2006).
- [11] Z. S. Wu, W. C. Ren, L. B. Gao, B. L. Liu, C. B. Jiang, and H. M. Cheng, Carbon **47** (2), 493 (2009).
- [12] G. D. Yuan, W. J. Zhang, Y. Yang, Y. B. Tang, Y. Q. Li, J. X. Wang, X. M. Meng, Z. B. He, C. M. L. Wu, I. Bello, C. S. Lee, and S. T. Lee, Chem. Phys. Lett. **67** (4-6), 361 (2009).
- [13] A. Dato, V. Radmilovic, Z. Lee, J. Phillips, and M. Frenklach, Nano Lett. **8** (7), 2012 (2008).
- [14] T. Ohta, A. Bostwick, T. Seyller, K. Horn, and E. Rotenberg, Science **313** (5789), 951 (2006).
- [15] E. McCann, Phys. Rev. B **74** (16), 161403 (2006).
- [16] E. Castro, K. Novoselov, S. Morozov, N. Peres, J. Dos Santos, J. Nilsson, F. Guinea, A. Geim, and A. Neto, Phys. Rev. Lett. **99** (21), 216802 (2007).
- [17] J. Oostinga, H. Heersche, X. Liu, A. Morpurgo, and L. Vandersypen, Nat. Mater. **7** (2), 151 (2007).
- [18] W. Yao, D. Xiao, and Q. Niu, Phys. Rev. B **77** (23), 235406 (2008).
- [19] R. M. Westervelt, Science **320** (5874), 324 (2008).
- [20] M. Freitag, Nat. Nano. **3** (8), 455 (2008).
- [21] J. C. Charlier, J. P. Michenaud, and X. Gonze, Phys. Rev. B **46** (8), 4531 (1992).
- [22] C. L. Lu, C. P. Chang, Y. C. Huang, J. M. Lu, C. C. Hwang, and M. F. Lin, J. Phys. Condens. Mat. **18** (26), 5849 (2006).
- [23] C. L. Lu, C. P. Chang, Y. C. Huang, R. B. Chen, and M. L. Lin, Phys. Rev. B **73** (14), 144427 (2006).
- [24] J. R. Huang, J. Y. Lin, B. H. Chen, and M. H. Tsai, Phys. Status Solidi B **245** (1), 136 (2008).
- [25] L. A. Falkovsky, J. Exp. Theor. Phys. **106** (3), 575 (2008).
- [26] K. F. Mak, M. Y. Sfeir, Y. Wu, C. H. Lui, J. A. Misewich, and T. F. Heinz, Phys. Rev. Lett. **101** (19) (2008).
- [27] Z. Q. Li, E. A. Henriksen, Z. Jiang, Z. Hao, M. C. Martin, P. Kim, H. L. Stormer, and D. N. Basov, Nat. Phys. **4** (7), 532 (2008).
- [28] C. Casiraghi, A. Hartschuh, E. Lidorikis, H. Qian, H. Harutyunyan, T. Gokus, K. S. Novoselov, and A. C. Ferrari, Nano Lett. **7** (9), 2711 (2007).
- [29] Z. Jiang, E. A. Henriksen, L. C. Tung, Y. J. Wang, M. E. Schwartz, M. Y. Han, P. Kim, and H. L. Stormer, Phys. Rev. Lett. **98** (19), 197403 (2007).
- [30] J. Yan, Y. Zhang, P. Kim, and A. Pinczuk, Phys. Rev. Lett. **98** (16), 166802 (2007).
- [31] Y. Zhang, T.-T. Tang, C. Girit, Z. Hao, M. C. Martin, A. Zettl, M. F. Crommie, Y. R. Shen, and F. Wang, Nature **459** (7248), 820 (2009).
- [32] F. Wang, Y. B. Zhang, C. S. Tian, C. Girit, A. Zettl, M. Crommie, and Y. R. Shen, Science **320** (5873), 206 (2008).
- [33] K. F. Mak, C. H. Lui, J. Shan, and T. F. Heinz, Phys. Rev. Lett. **102** (25), 256405 (2009).
- [34] Y. Xu, X. Li, and J. Dong, Nanotechnology **21**, 065711 (2010).
- [35] W. Norimatsu and M. Kusunoki, Phys. Rev. B **81** (16), 161410(R) (2010).
- [36] K. F. Mak, J. Shan, and T. F. Heinz, Phys. Rev. Lett. **104** (17), 176404 (2010).
- [37] A. H. Castro Neto, F. Guinea, N. M. R. Peres, K. S. Novoselov, and A. K. Geim, Rev. Mod. Phys. **81** (1), 109 (2009).
- [38] F. Guinea, A. H. Castro Neto, and N. M. R. Peres, Solid State Commun. **143** (1-2), 116 (2007).
- [39] J. L. Manes, F. Guinea, M. A. H. Vozmediano, Phys. Rev. B **75** (15), 155424 (2007).
- [40] M. F. Craciun, S. Russo, M. Yamamoto, J. B. Oostinga, A. F. Morpurgo, and S. Thruha, Nat. Nano. **4** (6), 383 (2009).
- [41] M. Aoki and H. Amawashi, Solid State Commun. **142** (3), 123 (2007).
- [42] H. K. Min and A. H. MacDonald, Phys. Rev. B **77** (15), 155416 (2008).
- [43] M. Koshino and E. McCann, Phys. Rev. B **80** (16), 165409 (2009).
- [44] M. Koshino, Phys. Rev. B **81** (12), 125304 (2010).
- [45] F. Zhang, B. Sahu, H. K. Min, and A. H. MacDonald, Phys. Rev. B **82** (3), 035409 (2010).
- [46] C. L. Lu, H. C. Lin, C. C. Hwang, J. Wang, M. F. Lin, and C. P. Chang, Appl. Phys. Lett. **89** (22), 221910 (2006).
- [47] C. P. Chang, J. Wang, C. L. Lu, Y. C. Huang, M. F. Lin, and R. B. Chen, J. Appl. Phys. **103** (10), 103109 (2008).
- [48] M. Gajdos, K. Hummer, G. Kresse, J. Furthmuller, and F. Bechstedt, Phys. Rev. B **73** (4), 45112 (2006).
- [49] G. Kresse and J. Hafner, Phys. Rev. B **48** (17), 13115 (1993).
- [50] D. M. Ceperley and B. J. Alder, Phys. Rev. Lett. **45** (7), 566 (1980).
- [51] P. E. Blochl, Phys. Rev. B **50** (24), 17953 (1994).
- [52] G. Kresse and D. Joubert, Phys. Rev. B **59** (3), 1758 (1999).
- [53] R. Haering, Can. J. Phys. **36** (3), 352 (1958).
- [54] Z. Q. Li, E. A. Henriksen, Z. Jiang, Z. Hao, M. C. Martin, P. Kim, H. L. Stormer, and D. N. Basov, Phys. Rev. Lett. **102** (3), 037403 (2009).
- [55] A. B. Kuzmenko, E. v. Heumen, D. v. d. Marel, P. Lerch, P. Blake, K. S. Novoselov, and A. K. Geim, Phys. Rev. B **79** (11), 115441 (2009).
- [56] F. Guinea, A. H. Castro Neto, and N. M. R. Peres, Phys. Rev. B **73** (24), 245426 (2006).
- [57] G. Ghosh, *Handbook of optical constants of solids: five-volume set.* (Academic Press, San Diego [etc.], 1998).